Numerical simulation of liquid sloshing in a baffled rectangular tank under irregular excitations

Zi-Hao Wang[a], Sheng-Chao Jiang[a,b,*], Wei Bai[c], Jin-Xuan Li[b]

[a]*School of Naval Architecture, Faculty of Vehicle Engineering and Mechanics, Dalian University of Technology, Dalian 116024, China*
[b]*State Key Laboratory of Coastal and Offshore Engineering, Dalian University of Technology, Dalian 116024, China*
[c]*Department of Computing and Mathematics, Manchester Metropolitan University, Chester Street, Manchester M1 5GD, UK*

Abstract

Sloshing responses in vertical and horizontal baffled tanks under irregular external excitations are investigated by employing a viscous fluid flow model with the Navier-Stokes solver. After the extensive validation of the present numerical model, the numerical experiment reveals many new understandings of the problem. A three-phase variation is suggested to describe the sloshing response under irregular excitations, that is, the first-order natural period controlling stage, the second-order natural period controlling stage, and the transitional stage between them. The sloshing periods are always around the corresponding natural periods with small standard deviations at the first- and second-order natural period controlling stages; while the decreased sloshing periods with large standard deviations can be observed at the transitional stage between them. The sloshing energy concentrated at a single natural frequency or multiple natural frequencies is the major reason for the phenomena. Compared to the results under regular excitations, smaller and larger sloshing amplitudes can be observed in the results of irregular excitations around the resonant and non-resonant frequency ranges, respectively. The normalised sloshing amplitudes calculated from the samplings of the large free surface amplitudes are always smaller than the samplings of the small free surface amplitudes.

Keywords: Sloshing, Irregular excitation, Vertical baffled tank, Horizontal baffled tank, Two-phase flow, Ramp function

1. Introduction

Liquid sloshing is a motion of water in partially filled storage under external excitations, which usually represents a kind of complex interface flows in a confined space. When the external excitation is of large amplitude or close to the sloshing natural frequency, the violent sloshing flow is able to produce a large impact pressure on the storage tank. Liquid sloshing widely occurs in the ocean and offshore engineering, such as in Floating Liquefied Natural Gas (FLNG) production systems, Liquefied Natural Gas (LNG) and Liquefied Petroleum Gas (LPG) carriers. The large-amplitude sloshing-induced forces can affect the global response of the liquid cargo ship. In addition, the local impact loading of the internal sloshing might cause damage to

*Corresponding author
Email address: jiangshengchao@foxmail.com (Sheng-Chao Jiang)

the tank wall. Therefore, investigations of liquid sloshing problems have a rather important academic value and wide engineering background.

The free surface nonlinearity is an important feature in the liquid sloshing behaviour, which has been studied by various methods, extensively. Based on the analytical method, Faltinsen and Timokha (2001, 2002) investigated the nonlinear liquid sloshing in a rectangular tank with a finite water depth by using the adaptive multi-radial approach and asymptotic modal approximation. Hill (2003) studied the transient evolution of the weakly nonlinear sloshing in a rectangular basin using the multiple-scales analysis. A fully nonlinear potential flow model was established by Wu et al. (1998) for simulating the sloshing wave in a three-dimensional tank based on the finite element method. Numerical simulations cover the standing waves, travelling waves and bores, and the occurrence of high pressures. A time-independent finite difference analysis was developed by Chen (2005) for analysing the fully nonlinear and viscous fluid sloshing flow motion in a rectangular tank, by which the influence of the Froude number and Reynolds number was discussed. Liu and Lin (2008) adopted the Volume of Fluid (VOF) method to simulate the three-dimensional liquid sloshing with a broken free surface, where the six degrees of freedom excitation in a non-inertial reference frame was considered. Rafiee et al. (2011) measured the sloshing phenomenon in a rectangular tank under the sway excitation in the laboratory test, in which the sloshing-induced impact pressure on the tank was studied.

In order to suppress the adverse effect of liquid sloshing phenomena, the use of baffles inside the tanks was proposed in several works. Cho et al. (2005) adopted the horizontal baffles to reduce the sloshing flow motion around the resonant frequency by using the linear potential flow model. A nonlinear potential flow model was developed by Biswal et al. (2006) for the sloshing response in a two-dimensional rectangular liquid chamber with a rigid baffle. The comparison of the numerical results between the linear and nonlinear potential flow models showed that the free surface nonlinearity plays an important role in the baffled sloshing problem. Liu and Lin (2009) investigated the suppressing effect of the vertical baffle on the sloshing flow motion based on the Navier-Stokes solver with the VOF technique. Akyıldız et al. (2013) conducted the laboratory test on the liquid sloshing in a rigid cylindrical tank with ring baffles. Lu et al. (2015) investigated the sloshing responses in the non-baffled and baffled tanks under an extremely long time-series excitation by using a Navier-Stokes solver. Numerical simulations suggested that the fully developed shear flow and vortex shedding can be induced by the baffle edge, which is the major reason for the physical energy dissipation. The influence of vertical baffles with different configurations on suppressing the sloshing pressure was studied by Xue et al. (2017), experimentally. Sanapala et al. (2018) and Chu et al. (2018) investigated the sloshing flow in the multiple horizontal and multiple vertical baffles, respectively. Jiang et al. (2022a,b) simulated the influence of internal baffles on suppressing the sway motion of the tank coupled with the internal sloshing flow under the wave action. Numerical simulations suggested that the proper baffle arrangements can reduce the sway-sloshing motion and make the ship sway amplitude similar to that without the sloshing effect. In addition to the rigid baffles, the perforated baffle can also reduce the liquid sloshing flow in the tank, as shown in the work of Molin and Remy (2013), Jin et al. (2017) and Yu et al. (2019), among others.

The above-mentioned work mainly focused on the sloshing responses under the regular excitation or regular wave action, whereas in reality, the storage tank may undergo irregular external excitations. Isaacson and Subbiah (1991) described the liquid sloshing in a rigid circular cylindrical tank subjected to the earthquake-induced excitations. A simplified method of estimating maximum forces using modal analysis and involving the earthquake response spectra was considered. Wang and Khoo (2005) simulated a two-dimensional random sloshing flow by using the fully nonlinear potential flow theory. It is found that the sloshing spectrum is mainly concentrated at the natural frequencies of the container, where the ith order natural frequency is dominant when the peak frequency is close to the ith order natural frequency. A fully nonlinear potential flow model was adopted by Sriram et al. (2006) to investigate the motion of sloshing flows under random excitations in the sway and heave modes. Numerical simulations showed that the peak value of the sloshing responses always appears at the natural frequencies under the sway excitations. In the case of random excitations in the vertical direction, the dominant peak value appears only in the first mode. Luo et al. (2016) adopted the consistent particle method to study the three-dimensional water sloshing under irregular translational and rotational excitations. Various wave patterns, including length-, width- and diagonal-dominant waves and swirling waves, were simulated. General speaking, the sloshing response under the irregular excitation shows more complex hydrodynamic behaviour than that under the regular excitation.

In this study, the behaviour of liquid sloshing in the baffled tank under irregular excitations is investigated numerically. It can be observed according to the discussion above that the previous work mainly focused on the spectral analysis of the sloshing flow when the baffled tank is under irregular excitations. However, not much light has been thrown on the statistical characteristics of the sloshing response in this problem, which is an important aspect of describing the irregular sloshing flow. The present numerical analysis includes the energy spectrum of the sloshing response, sloshing amplitudes by different statistic samplings, histogram of sloshing amplitudes and periods, variation of sloshing periods and corresponding standard deviations. New understandings of the sloshing flow induced by the irregular excitation in a rectangular tank are created and the physical mechanisms behind the sloshing response are revealed, which is the primary motivation of this study.

2. Mathematical Formulation

The Navier-Stokes equations for the incompressible two-phase viscous fluid flow in the Arbitrary Lagrangian - Eulerian (ALE) reference system can be written as follows,

$$\frac{\partial \rho}{\partial t} + \frac{\partial \rho u_i}{\partial x_i} = 0 \tag{1a}$$

$$\frac{\partial \rho u_i}{\partial t} + \frac{\partial \rho (u_j - u_j^m) u_i}{\partial x_j} = \rho g_i - \frac{\partial p}{\partial x_i} + \mu_e \frac{\partial}{\partial x_j}\left(\frac{\partial u_i}{\partial x_j} + \frac{\partial u_j}{\partial x_i}\right) \tag{1b}$$

where u_i denotes the velocity component in the ith direction; u_j^m denotes the velocity component due to the mesh deformation in the ALE frame. g_i and p are the gravitational acceleration and pressure, respectively.

ρ and μ are the fluid density and fluid dynamics viscosity.

The Volume of Fluid (VOF) method (Hirt and Nichols, 1981) is used to capture the free surface motion. The fractional function φ is defined as,

$$\varphi = \begin{cases} 0, & \text{in the air} \\ 0 < \varphi < 1, & \text{on the free surface} \\ 1, & \text{in the water} \end{cases} \tag{2}$$

It satisfies the advection equation,

$$\frac{\partial \varphi}{\partial t} + (u_i - u_i^m)\frac{\partial \varphi}{\partial x_i} = 0 \tag{3}$$

The fluid density and dynamic viscosity of the two-phase flow can be determined according to the fluid phase function as follows,

$$\rho = \varphi\rho_W + (1-\varphi)\rho_A \tag{4a}$$

$$\mu_e = \varphi\mu_{eW} + (1-\varphi)\mu_{eA} \tag{4b}$$

where the subscripts W and A represent the properties in Water phase and Air phase, respectively. In numerical simulations, the contour of VOF function with $\varphi = 0.5$ is taken as the free surface elevation.

The finite volume method (FVM) is used to discretize the governing equations (1a)-(1b) and the VOF equation (3). The time discretization is in the Eulerian format, and the scatter and gradient calculations are in the Gauss Vanleer and Gauss linear formats, respectively. The diffusion term is approximated using Gauss linear corrected format. The Navier-Stokes equations are solved by the PISO (Pressure Implicit with Splitting of Operators) method (Issa, 1986). The Euler method is used to discretize the transient term. The convection term and diffusion term are discretized by the Gauss Limited Linear method and the Gauss Linear Corrected method, respectively. The time increment in numerical simulations is automatically determined according to the Courant-Friedrichs-Lewy (CFL) condition,

$$\Delta t \leq C_r \times \min\{\sqrt{S_e}/|u_e|\} \tag{5}$$

where S_e and $|u_e|$ are the area and absolute velocity in a computational cell, respectively. In the calculation, the Courant number C_r is taken as 0.2 to ensure the computational stability and numerical accuracy. For more information on the numerical method and implementation in the OpenFOAM® package, please refer to Jasak (1996) and Rusche (2003).

The simulations are conducted at the Supercomputer Center of Dalian University of Technology by using the OpenFOAM® package with version 3.0.0. Numerical simulations start from the still state, where the hydrostatic pressure and zero velocity are specified as the initial conditions. The no-slip boundary condition $u_i = U$ is imposed on the solid wall. At the upper centre of the sloshing tank, a reference pressure $p = 0$ is implemented.

3. Numerical Setup and Validation

As shown in Fig. 1, three types of sloshing tanks, that is, non-baffled tank, vertical baffled tank and horizontal baffled tank, are selected in this study. Noted that the present work is based on the two-dimensional numerical simulation and the rectangular tank with breadth B is partially filled with water in depth H. Numerical validations are carried out for the non-baffled tank in Fig. 1a, firstly, where the geometry with B = 1.0 m and H = 0.5 m is considered. For a rectangular tank with a given breadth and filling depth, the n-order natural frequency ω_n of the liquid sloshing response in the tank can be calculated from the theoretical equation derived by Faitinsen et al. (1978) as,

$$\omega_n = \sqrt{g k_n \tanh(k_n H)}, \quad k_n = (2n-1)\pi/B, \quad n = 1, 2, \cdots, \tag{6}$$

where ω_n and k_n represent the angular frequency and wave number, respectively. In this study, the first-order natural frequency of liquid sloshing in the rectangular tank without baffles is ω_1 = 5.314 rad/s.

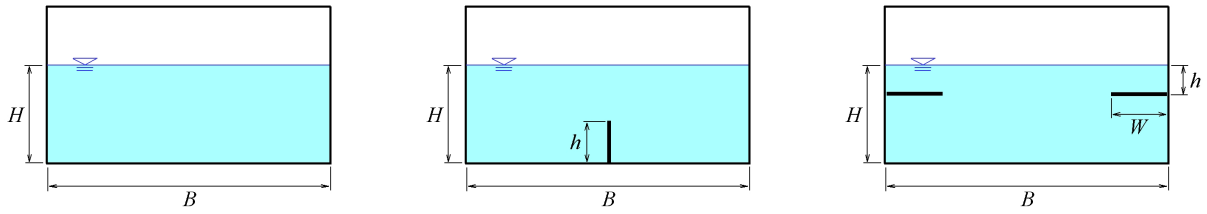

(a) Non-baffled tank (b) Vertical baffled tank (c) Horizontal baffled tank

Figure 1: Sketch of the definition of geometries of sloshing tanks.

The sinusoidal function is adopted as the displacement of the horizontal excitation as follows,

$$x(t) = b \sin \omega_e t \tag{7}$$

where b and ω_e are the exciting amplitude and angular frequency, respectively. Convergent tests are firstly carried out for the present numerical model, where the geometries and external excitations are illustrated in Tab. 1. For each case, three runs with different mesh resolutions are conducted, namely, M1, M2 and M3, respectively. The coarse mesh M1 comprises 10000-16000 computational cells while the fine mesh M3 comprises 60000 - 80000 cells. More detailed discretization schemes and the mesh generation can refer to Jiang et al. (2022a,b). Refined meshes are generated in the regions close to the free surface and internal baffles. The numerical results of the stable sloshing amplitude along the right-side wall with various mesh resolutions are also presented in Tab. 1. It can be seen that the stable amplitudes for each case are in good agreement. The relative error between the coarse mesh M1 and the fine mesh M4 does not exceed 8% in those four cases. To ensure numerical accuracy and save computational time, the medium mesh M2 is adopted for the computations in this work.

Table 1: Convergent test with various mesh resolutions.

Case	b (m)	ω_e (rad/s)	Vertical baffle	Horizontal baffles		η_A (mm)	Error (%)
			h/H	W/B	h/H		
Case 1	0.01	2.655	None	None	None	M1: 4.65 M2: 4.90 M3: 4.91	5.30 0.20
Case 2	0.0004	5.048	None	None	None	M1: 4.63 M2: 4.86 M3: 4.90	5.51 0.82
Case 3	0.002	4.15	0.80	None	None	M1: 27.53 M2: 26.20 M3: 25.62	7.44 2.26
Case 4	0.002	4.21	None	0.40	0.40	M1: 9.72 M2: 9.27 M3: 9.27	4.83 0.04

Two sets of excitation cases, that is, $b = 0.01$ m with $\omega_e = 0.50\ \omega_1$ and $b = 0.0004$ m with $\omega_e = 0.95\ \omega_1$, are adopted for validations in this study. Time histories of the free surface evolutions at the right side of the tank are compared with the analytical solution in Faitinsen et al. (1978) based on the potential flow theory and the numerical results in Liu and Lin (2008) by using a viscous fluid flow model, as shown in Fig. 2. It can be seen from the figure that the linear potential flow solutions only agree well with two viscous fluid flow results at the early stage of the external excitation between 0-10 s. With the elapse of time, the potential flow solutions have an evident difference from the viscous fluid model results. The sloshing amplitudes predicted by the potential fluid model are generally larger than those predicted by the viscous fluid model, and the over-prediction is mainly due to the neglect of the fluid viscosity and flow rotation in the potential flow theory. In Fig. 2a, the discrepancy is only seen in the wave crest and wave trough; while in Fig. 2b, a slight increase in the sloshing flow period can also be observed in the viscous fluid flow model compared to that in the analytical solutions. The relevant studies in Antuono and Colagrossi (2013) suggested that the fluid viscosity can affect the dispersion relation of water waves and enlarge the wave period. Finally, two viscous fluid flow results are in good agreement with each other, indicating the present numerical model can work well in predicting the non-baffled sloshing problem.

Furthermore, the sloshing response in the vertical baffled tank is validated, where a vertical baffle is applied at the centre of the tank and mounted on the bottom, as shown in Fig. 1b. The geometry of $B = 1.0$ m and $H = 0.5$ m with a baffle height of $h/H = 0.75$ is adopted, where the external excitation is of $b = 0.002$

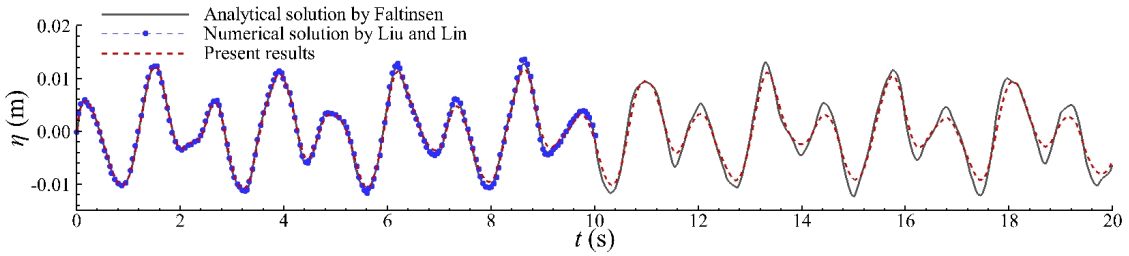

(a) $b = 0.01$ m, $\omega_e = 0.50\ \omega_1$

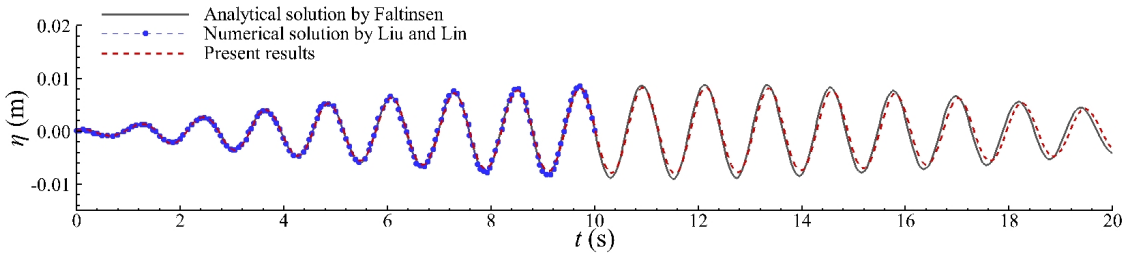

(b) $b = 0.0004$ m, $\omega_e = 0.95\ \omega_1$

Figure 2: Comparison of time histories of the free surface at the right side of the non-baffled tank.

m and $\omega_e = 5.29$ rad/s. The numerical results of the free surface at the right side of the vertical baffled tank are shown in Fig. 3, and compared with the CFD results in Liu and Lin (2009). Good agreement between two numerical results can be observed, validating the reliability of the numerical model in this study.

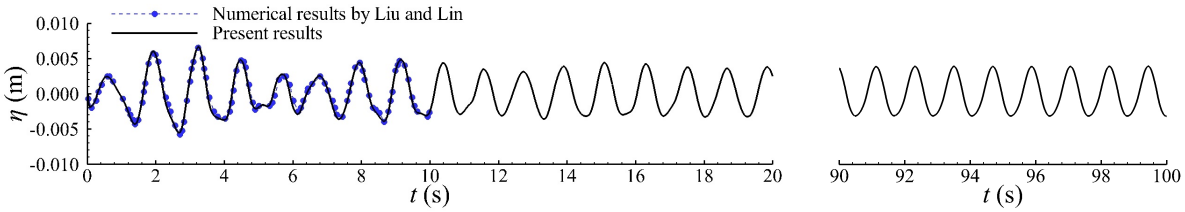

Figure 3: Comparison of time histories of the free surface at the right side of the vertical baffled tank.

Finally, the numerical validation is extended to the sloshing flow in the horizontal baffled tank in Fig. 1c. The CFD results in Xue and Lin (2011) and Belakroum et al. (2010) for a tank with the breadth $B = 0.9$ m and filling depth $H = 0.6$ m are adopted for the comparison, where the baffle breadth $W/B = 0.225$ and submerged depth $h/H = 0.50$ under the excitation of $b = 0.00198$ m and $\omega_e = 5.40$ rad/s are considered. General speaking, the present numerical model can work well in predicting the horizontal baffled sloshing response, as illustrated in Fig. 4. According to the comparison of the numerical simulations in this section, it is found that the present numerical model is able to produce accurate results in the liquid sloshing problem with and without baffles, which can be adopted in the following simulations.

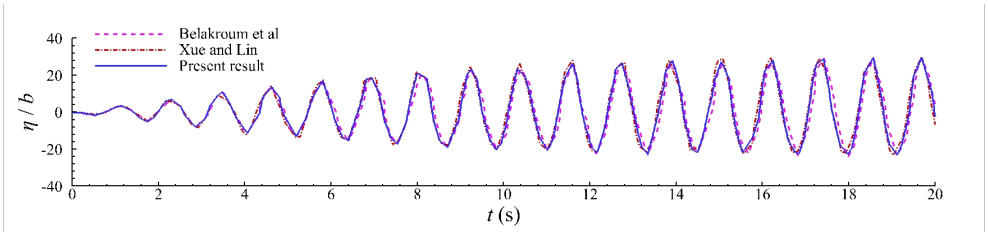

Figure 4: Comparison of time histories of the free surface at the right side of the horizontal baffled tank.

4. Liquid Sloshing under Regular Excitation

The geometries introduced in Figs. 1b and 1c are employed in the numerical simulations in this section, where the parameters of the tank are tabulated in Tab. 2, and the excitation amplitude is $b = 0.002$ m in all the cases. To avoid the transient effect and save the computational time, a ramp function is adopted in the starting time of the external sinusoidal excitation, that is,

$$x(t) = R_m(t) \cdot bsin\omega_e t \tag{8}$$

where $R_m(t)$ is the ramp function as follows,

$$R_m(t) = \begin{cases} \frac{1}{2}\left[1 - \cos\left(\frac{\pi t}{T_m}\right)\right], & t < T_m \\ 1, & t > T_m \end{cases} \tag{9}$$

and T_m indicates the ramp time, and is taken as $T_m = 10T_e$ in this study. To demonstrate the effect of the ramp function on the numerical results, the sloshing flows in the vertical baffled tank with $h/H = 0.4$ and the horizontal baffled tank with $W/B = 0.2$ and $h/H = 0.8$ are adopted, where the first-order natural frequencies are $\omega_1^v = 5.08$ rad/s and $\omega_1^h = 5.28$ rad/s, respectively. The sloshing responses without and with the ramp function, that is, excited by Eqs. (7) and (9), are compared in Fig. 5 when the excitation frequencies are far from the natural frequencies at $\omega_e = 0.65\omega_1^v = 3.30$ rad/s and $\omega_e = 0.65\omega_1^h = 3.43$ rad/s. The significant transient can be observed before $t = 100$ s in the results without the ramp function, while the steady-state sloshing evolutions can be obtained after $t = 30$ s when the ramp function is employed. In the present simulations, the computer time is around 1.40 and 1.43 hours for the vertical and horizontal baffled tanks with the ramp function; while they become 6.83 and 8.53 hours for the cases without the ramp function. Noted that the computational resource of 6* Intel(R) Core(TM) i5-10500 CPU @ 3.10GHz is adopted in this study. This implies that the ramp function is able to generate the steady-state results more rapidly when the excitation frequency is far from the resonant frequency. Therefore, the ramp function can significantly improve the simulation in non-resonant conditions.

Fig. 6 illustrates the influence of the ramp function when the excitation frequency is close to the natural frequency. In difference to the non-resonant frequency results, the ramp function cannot avoid the initial transit at the natural frequency. The comparison indicates that the initial transit is delayed by the ramp function, and the steady-state evolution is obtained more slowly when the ramp function is equipped. Around

Table 2: Parameters of the vertical and horizontal baffled tanks in this study.

Parameters	Value
Breadth of the rectangular tank, B	1.0 m
Filling depth in the tank, H	0.5 m
Dimensionless breadth of the horizontal baffle, W/B	0.2 / 0.3 / 0.4
Distance of the horizontal baffle from the free surface, h/H	0.2 / 0.3 / 0.4
Height of the vertical baffle, h/H	0.2 / 0.3 / 0.4

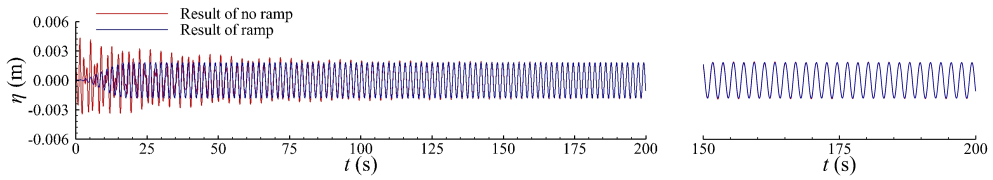

(a) Vertical baffle

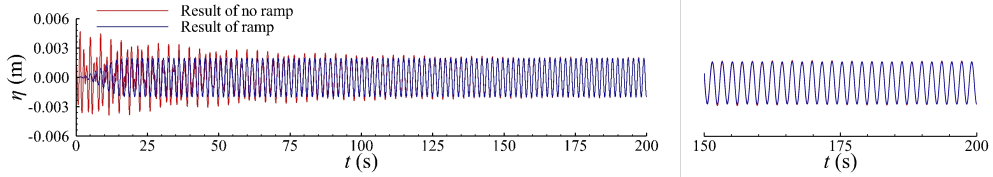

(b) Horizontal baffle

Figure 5: Time histories of the free surface elevations at the right wall of the tank when the excitation frequency is $\omega_e = 0.65\omega_1^v$ and $\omega_e = 0.65\omega_1^h$.

the resonant frequency, the free surface amplitude increases with the elapse of time, which is the process of energy accumulation. The allocation of the ramp function delays the energy accumulation, which is the major reason for the above delay phenomenon. Therefore, it is unnecessary to use the ramp function in resonant conditions. The comparison of the results between 150 - 200 s also indicates that the steady-state sloshing evolutions are independent of the ramp function, both at the non-resonant and resonant frequencies as shown in Figs. 5 and 6. Finally, it should be noted that the influence of the ramp function on the sloshing response is also insensitive for other excitation amplitudes, according to the numerical experiment in this study.

The sloshing behaviour in various baffled tanks under the regular sinusoidal excitations is examined, where the sloshing amplitudes are computed from the averaged free surface amplitudes during the steady-state evolutions. In the numerical simulations, the excitation amplitude $b = 0.002$ m is still adopted, while the excitation frequency varies in the range of 0 - 8 rad/s. Fig. 7a illustrates the influence of the vertical baffle height on the sloshing amplitude in the tank. Numerical simulations suggest that both the resonant frequency and resonant amplitude decrease with the increase of the relative baffle height h/H, implying

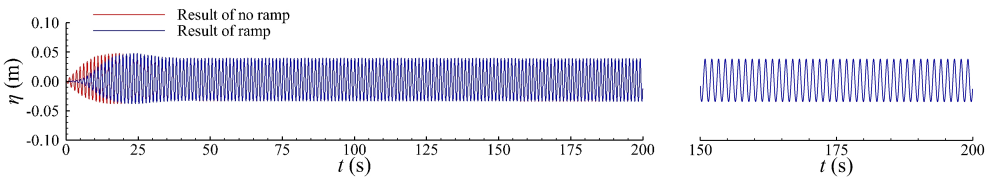

(a) Vertical baffle

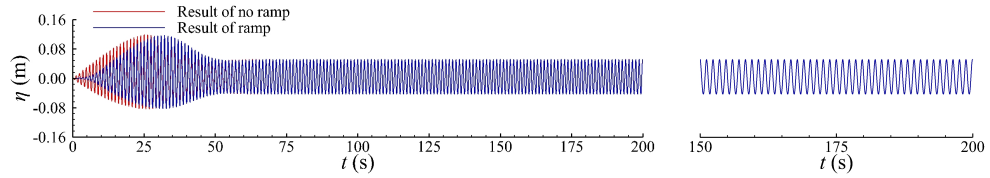

(b) Horizontal baffle

Figure 6: Time histories of the free surface elevations at the right wall of the tank when the excitation frequency is $\omega_e = 1.0\omega_1^v$ and $\omega_e = 1.0\omega_1^h$.

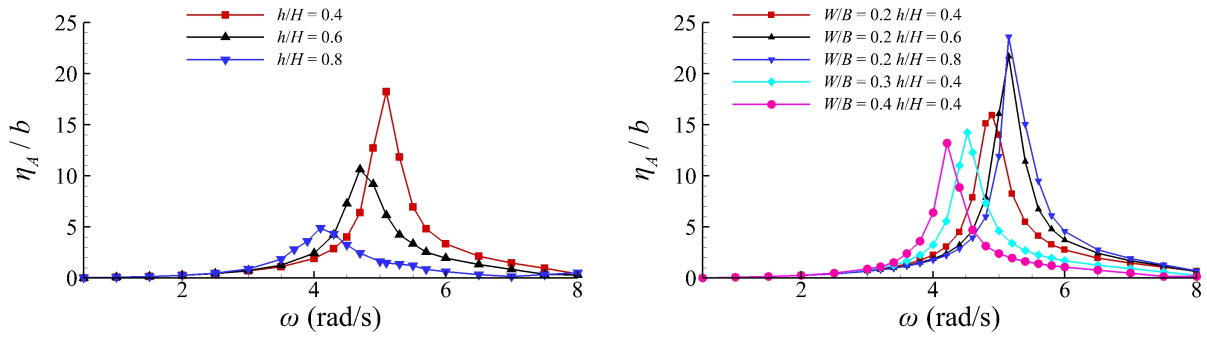

(a) Vertical baffle

(b) Horizontal baffles

Figure 7: Influence of the baffle geometry on the sloshing response under regular excitations at different frequencies.

that the vertical baffle with a large height can suppress the sloshing response, more effectively. As for the sloshing response in the horizontal baffled tank in Fig. 7b, the decreased resonant frequency and resonant amplitude can be obtained by the larger baffle breadth W/B and smaller relative baffle depth h/H. The above conclusions are similar to those in the previous literature for sloshing flows under regular sinusoidal excitations, such as Lu et al. (2015) and Xue et al. (2017).

5. Liquid Sloshing under Irregular Excitation

5.1. Generation of irregular excitation

In order to examine the sloshing response under the irregular excitation, a time history of the irregular external oscillation needs to be generated, firstly. The irregular oscillation can be modelled in a stochastic

way by the sum of a large number of independent linear cosine excitations as follows,

$$x(t) = \sum_{i=1}^{N_\omega} b_i \cos(\tilde{\omega_i} t + \tilde{\varphi_i}) \tag{10}$$

where $x(t)$ denotes the horizontal excitation displacement of the tank and N_ω is the number of all linear cosine excitations, which is $N_\omega = 200$ in this study. b_i, $\tilde{\omega_i}$ and $\tilde{\varphi_i}$ are the ith amplitude, angular frequency and phase shift of each cosine excitation, respectively. The excitation amplitude b_i can be obtained by the following equation (Yu and Liu, 2016),

$$b_i = \sqrt{2S(\tilde{\omega_i})\Delta\omega} \tag{11}$$

where $\Delta\omega$ denotes the frequency interval; $S(\tilde{\omega_i})$ is the displacement spectrum of the horizontal excitation. The values of $\tilde{\omega_i}$ and $\tilde{\varphi_i}$ include the random numbers, which can be written as,

$$\tilde{\omega_i} = (i - 1 + \varepsilon)\Delta\omega \tag{12a}$$

$$\tilde{\varphi_i} = 2\pi\varepsilon \tag{12b}$$

where ε is a random number, which is uniformly distributed in the interval $[0, 1]$.

The JONSWAP wave spectrum is adopted as the displacement spectrum $S(\omega)$ for the horizontal excitation,

$$S(\omega) = \alpha g^2 \frac{1}{\omega^2} \exp\left[-\frac{5}{4}\left(\frac{\omega_p}{\omega}\right)^4 \gamma^{\exp\left[-(\omega_p/\omega)^2/(2\sigma^2\omega_p^2)^2\right]}\right] \tag{13}$$

where ω and ω_p are the wave frequency and peak frequency, respectively. $\sigma = 0.07$ and 0.09 when $\omega < \omega_p$ and $\omega > \omega_p$, respectively. g is the acceleration due to gravity. $\gamma = 3.3$ is the peak enhancement factor for the mean JONSWAP spectrum. By adjusting the parameters α and ω_p, the expected significant wave height H_s and peak frequency ω_p can be obtained, which are adopted as the controlling parameters of irregular external excitations. In this study, the external exciting amplitude is taken as $b_s = H_s$ / 2. Finally, the ramp function is adopted again for avoiding the transit effect during the early stage of the excitation.

5.2. Characteristics of liquid sloshing response under irregular excitation

The vertical baffled tank with $h/H = 0.8$ and the horizontal baffled tank with $W/B = 0.4$ and $h/H = 0.4$ are adopted in this section. According to the CFD results under the regular excitation in Fig. 7, the corresponding frequency of the maximal free surface amplitude is $\omega_r = 4.20$ rad/s for these two baffled tanks. Free decay tests are conducted using the CFD simulations, by which the first- and higher-order sloshing natural frequencies can be obtained, as shown in Tab. 3. Our major objective is to study the hydrodynamic behaviour of the sloshing response under irregular external excitations. The excitation amplitude $b_s = 0.002$ m with three peak frequencies, that is, $\omega_p = 0.5\omega_r$, $1.0\omega_r$, $1.5\omega_r$ are selected in the numerical simulations. Time history of the free surface evolution along the right side of the tank with the peak frequency $\omega_p = \omega_r = 4.20$ rad/s is shown in Fig. 8. Irregular characteristics can be observed in the sloshing response results.

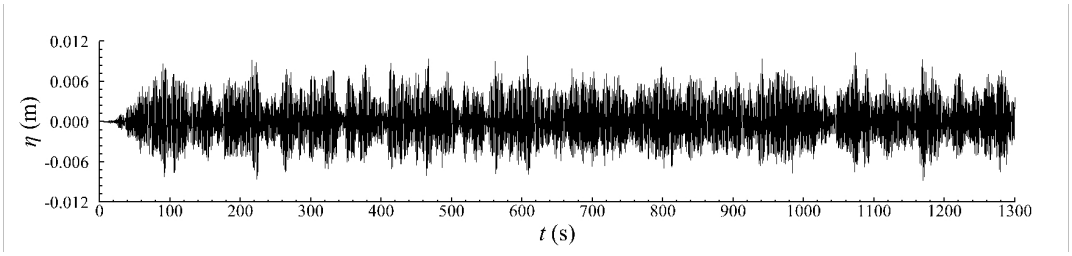

(a) Vertical baffled tank

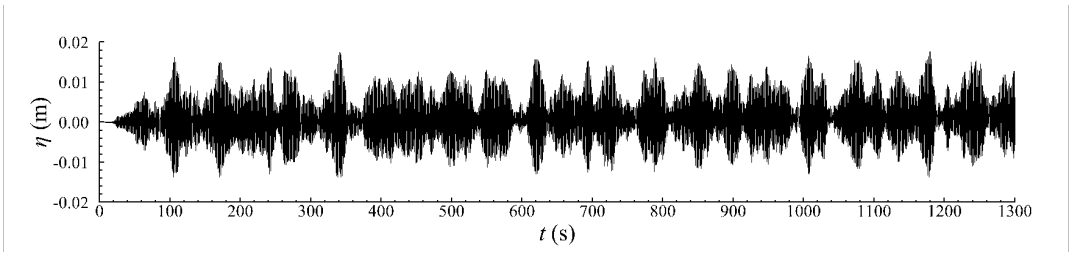

(b) Horizontal baffled tank

Figure 8: Time histories of the free surface at the right side of the tanks under the irregular excitation.

General speaking, the steady-state liquid sloshing response in the statistical sense can be observed after 100 s. Time window analysis also indicates that the statistical sloshing amplitudes between 100 - 500 s and 500 - 900 s are almost identical, which is suitable for both the vertical and horizontal baffled tanks. Therefore, the numerical results between 100 - 500 s are selected for the following analysis.

Table 3: Sloshing natural frequencies and periods of vertical and horizontal baffled tanks.

Parameters		Natural frequency (rad/s)	Natural Period (s)
Vertical baffled tank	1st-order	$\omega_1^v = 4.15$	$T_1^v = 1.51$
	2nd-order	$\omega_2^v = 9.43$	$T_2^v = 0.67$
	3rd-order	$\omega_3^v = 12.32$	$T_3^v = 0.51$
	4th-order	$\omega_4^v = 14.54$	$T_4^v = 0.43$
Horizontal baffled tank	1st-order	$\omega_1^h = 4.21$	$T_1^h = 1.49$
	2nd-order	$\omega_2^h = 9.43$	$T_2^h = 0.67$
	3rd-order	$\omega_3^h = 12.32$	$T_3^h = 0.51$
	4th-order	$\omega_4^h = 14.54$	$T_4^h = 0.43$

The behaviour of the sloshing response in two baffled tanks under the irregular external excitations is considered. As mentioned above, the amplitudes $b_s = 0.002$ m with three peak frequencies, that is, $\omega_p = 0.5\omega_r$, $1.0\omega_r$, $1.5\omega_r$, are adopted in the simulations. Fig. 9 shows the histograms for the amplitudes and periods of sloshing responses at the right wall of the vertical and horizontal baffled tanks, respectively. The

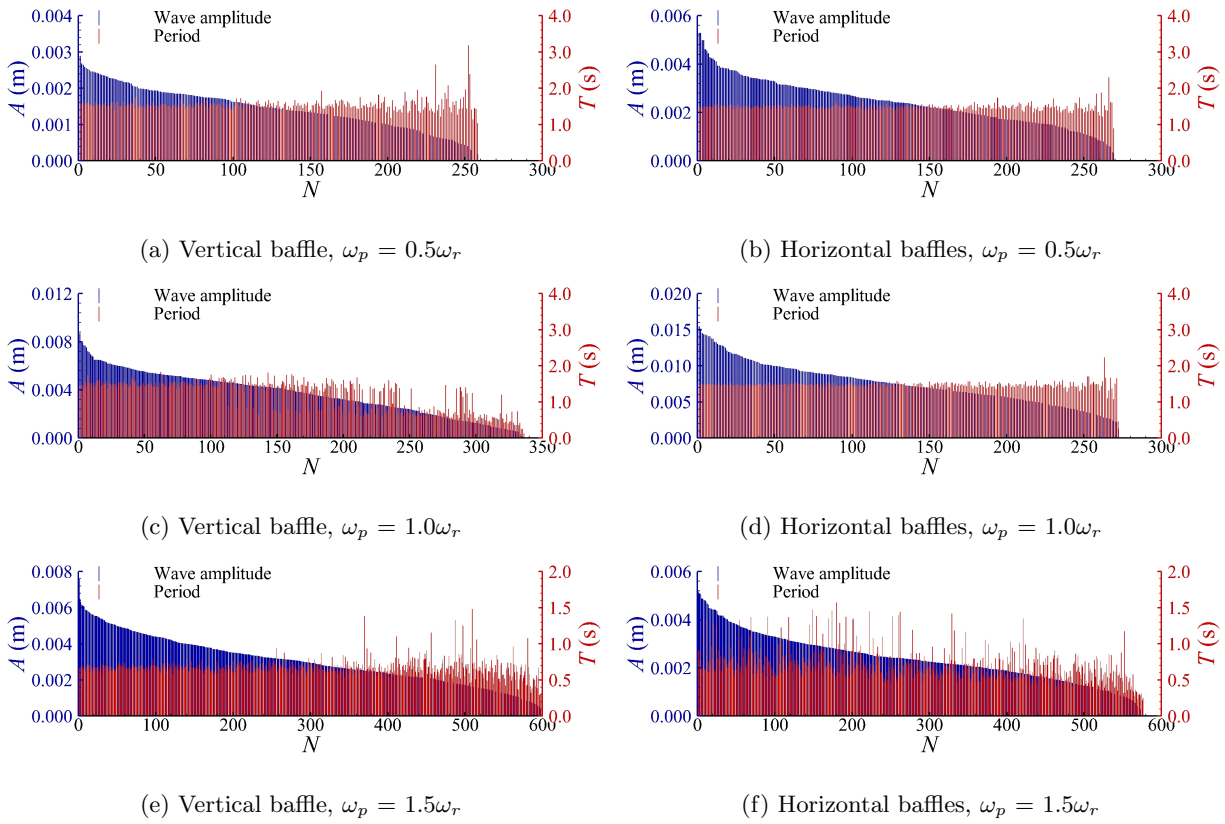

(a) Vertical baffle, $\omega_p = 0.5\omega_r$

(b) Horizontal baffles, $\omega_p = 0.5\omega_r$

(c) Vertical baffle, $\omega_p = 1.0\omega_r$

(d) Horizontal baffles, $\omega_p = 1.0\omega_r$

(e) Vertical baffle, $\omega_p = 1.5\omega_r$

(f) Horizontal baffles, $\omega_p = 1.5\omega_r$

Figure 9: Histograms of the free surface at the right side of the tanks under the irregular excitation.

wave amplitudes and corresponding periods are counted by using the zero up-crossing method, which are arrayed in a descending order of wave amplitudes in the figure. The x-axis of the figure is the series number of the sloshing wave N; while the y-axis is the wave amplitude and period in blue and red colours, respectively. The corresponding energy spectrums by the fast Fourier transform (FFT) method are illustrated in Fig. 10. In Figs. 9a and 9b, the free surface periods under the excitation of $\omega_p = 0.5\omega_r$ are mainly around $T = 1.54$ s and 1.49 s for the vertical and horizontal baffled tanks, which are in accordance with the first-order sloshing natural frequencies $\omega_1^v = 4.15$ rad/s and $\omega_1^h = 4.21$ rad/s, respectively. However, there is no corresponding sloshing response frequency around the peak frequency of the external excitation. The above results can also be demonstrated by the energy spectrum results in Figs. 10a and 10b. Generally, the behaviour of the wave heights and wave periods in the vertical and horizontal baffled tanks is very similar in terms of frequency at this excitation frequency.

In difference to the results at $\omega_p = 0.5\omega_r$, the sloshing responses under the irregular excitations with $\omega_p = 1.0\omega_r$ and $1.5\omega_r$ in the vertical and horizontal baffled tanks show the different characteristics in Figs. 9c - 9f. The sloshing periods in the vertical baffled tank are mainly around $T = 1.44$ s and 0.67 s in Fig. 9c. These are around the first- and second-order sloshing natural frequencies $\omega_1^v = 4.53$ and $\omega_2^v = 9.61$ rad/s, respectively. In Fig. 9d, the sloshing periods mainly appear around $T = 1.47$ s, which is the first-order

sloshing frequency $\omega_1^h = 4.21$ rad/s of the horizontal baffled tank. Correspondingly, the FFT analysis in Figs. 10c and 10d indicates the double-peak and single-peak spectrums for the vertical and horizontal baffled tanks, respectively. As for the results under the irregular excitation $\omega_p = 1.5\omega_r$, the dominant period around $T = 0.66$ s can be identified in both the vertical and horizontal baffled tanks. However, the multiple-period characteristic appears in the whole histogram for the horizontal baffled sloshing response in Fig. 9f and the lower one-half of the vertical baffled sloshing response in Fig. 9e. The above phenomena can be confirmed by the multiple-peak spectrum in Figs. 10e and 10f. The further comparison indicates that the corresponding frequencies of the spectral peaks are always around the sloshing natural frequencies, which applies to both the vertical and horizontal baffled tanks. According to the analysis in Figs. 9 and 10, it can be summarised that the sloshing responses under irregular excitations always oscillate around the sloshing natural frequencies. The variation of response periods for different peak frequencies or baffled types is mainly due to the activation of the single or multiple natural frequencies.

The sloshing response amplitudes in the vertical and horizontal baffled tanks under irregular excitations with different peak frequencies are shown in Fig. 11. The external excitation amplitude is still $b_s = 0.002$ m, and the range of external excitation peak frequencies is 0 - 8.0 rad/s. For the purpose of comparison, the sloshing responses under the regular excitation are also included in the figure, where the exciting amplitude is $b = 0.002$ m. The sloshing response amplitudes by irregular excitations are smaller than those by regular excitations around the resonant frequency. Around the non-resonant frequencies, the irregular excitation results are larger than the regular excitation results, especially at the scope of the high-frequency range. In the results of irregular excitations, the maximal sloshing amplitude can be obtained when the peak frequency is close to the natural frequency, which is the reason that more wave energy is distributed around the natural frequency. Furthermore, different statistical sloshing response amplitudes are compared in the irregular excitation results. Note that the normalised amplitudes are illustrated in these figures, where the normalisation is conducted by the corresponding statistical data, such as A_{max} / b_{max}, $A_{1/3}$ / $b_{1/3}$, A_{ave} / b_{ave}, and so on. It can be observed from these figures that the statistical results between $A_{1/3}$ and $A_{13\%}$ agree well with each other, implying that the sloshing response conforms to the statistical characteristics of the Rayleigh distribution. The normalised sloshing amplitudes computed by the samplings with large free surface amplitudes are always smaller than that by the samplings with small free surface amplitudes. That is, the values of $A_{1/10}$ / $b_{1/10}$ are smaller than $A_{1/3}$ / $b_{1/3}$; and the largest and smallest normalised sloshing amplitudes can be observed in the results of A_{ave} / b_{ave} and A_{max} / b_{max}, respectively. It can be understood that larger sloshing amplitude may generate more dissipation in the baffled tank. The above results also apply to both the vertical and horizontal baffled sloshing problems.

Fig. 12 shows the comparisons of sloshing amplitudes between the vertical and horizontal baffled tanks, including the regular and irregular external excitations. Under the regular excitation, the difference in the free surface amplitudes between the two liquid tanks is mainly around the resonance frequency, that is, ω = 3.8 - 5.0 rad/s in the figure. General speaking, the sloshing amplitudes in the vertical baffled tank are

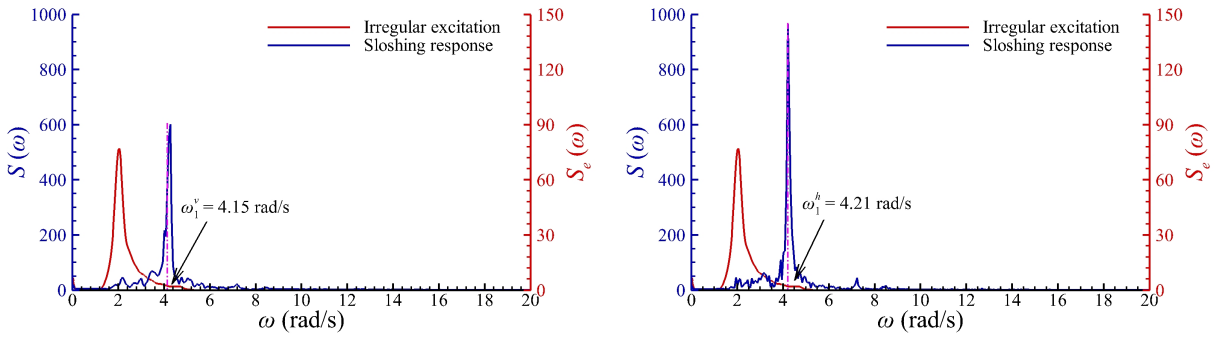

(a) Vertical baffle, $\omega_p = 0.5\omega_r$

(b) Horizontal baffles, $\omega_p = 0.5\omega_r$

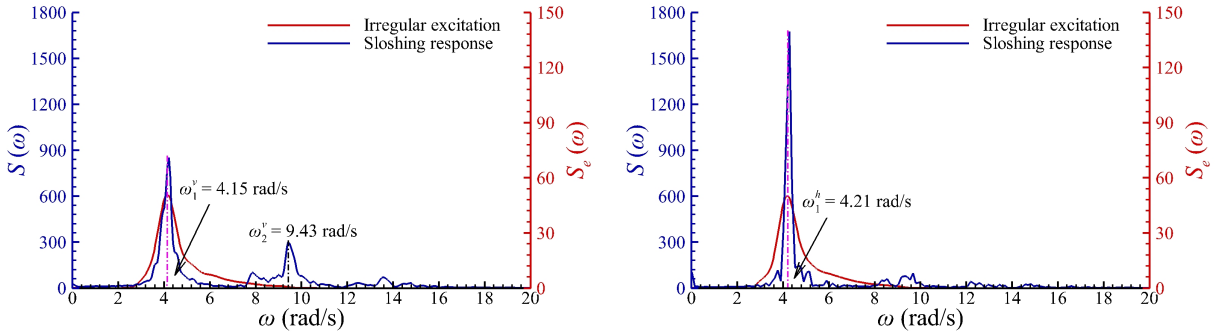

(c) Vertical baffle, $\omega_p = 1.0\omega_r$

(d) Horizontal baffles, $\omega_p = 1.0\omega_r$

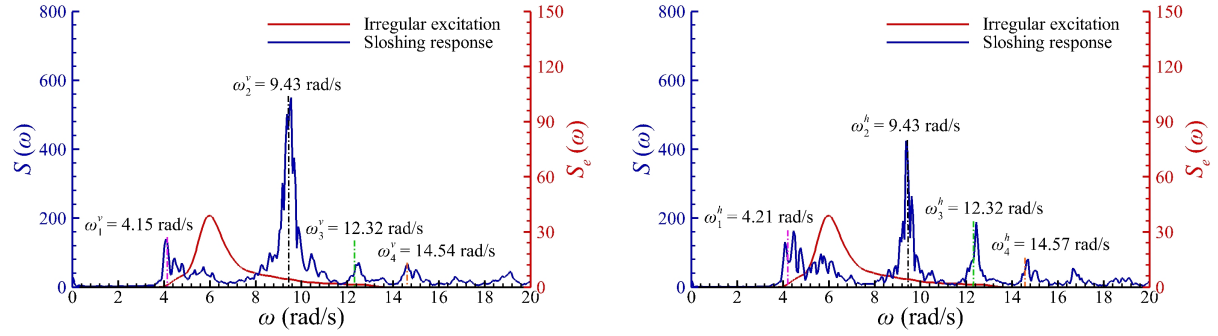

(e) Vertical baffle, $\omega_p = 1.5\omega_r$

(f) Horizontal baffles, $\omega_p = 1.5\omega_r$

Figure 10: Energy spectrum of the free surface at the right side of the tanks under the irregular excitation.

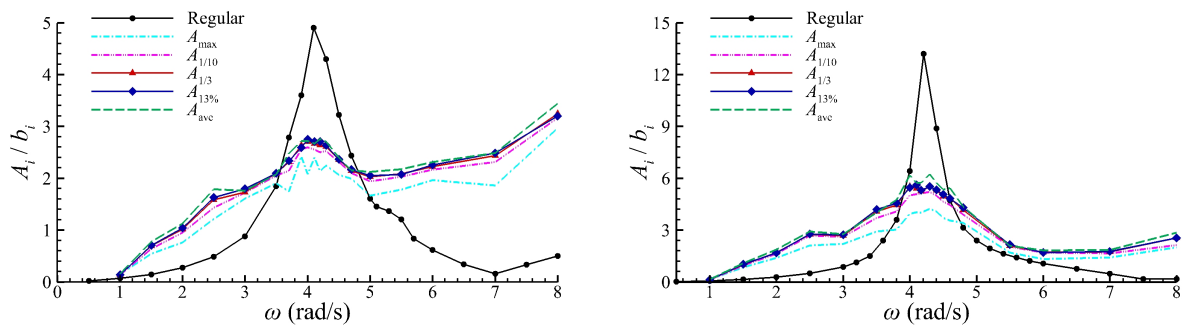

(a) Vertical baffles (b) Horizontal baffles

Figure 11: Comparison of sloshing response amplitudes between different statistics.

smaller than that in the horizontal baffled tank. In difference to the regular excitation results, the significant difference between the two baffled tanks can be observed at a wider frequency range, that is, from 2.0 to 5.5 rad/s, in the irregular excitation results. In addition, the sloshing amplitudes in the vertical baffled tank are larger than that in the horizontal baffled tank when the peak frequency is $\omega_p > 5.5$ rad/s, which is different from the regular excitation results under the exciting frequency $\omega > 7.5$ rad/s. The higher-order mode resonance induced by the irregular excitations may be the major reason for the phenomenon. The above results indicate that the behaviour of the sloshing response by irregular excitations has a significant difference from that of the regular excitations.

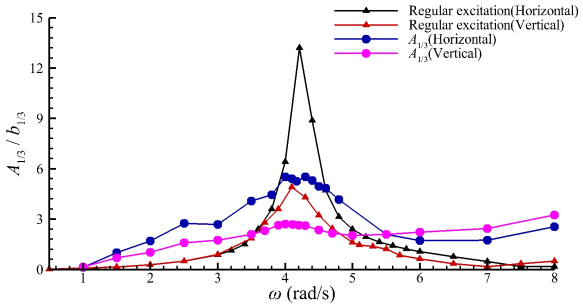

Figure 12: Comparison of amplitude-frequency response under regular and irregular excitations.

Finally, the variation of the sloshing response periods against the peak frequency of the irregular excitations is investigated. Fig. 13 shows the significant excitation periods $T_{1/3}$ of the sloshing response in the vertical and horizontal baffled tanks, respectively, including the corresponding standard deviations. A three-phase variation of the sloshing response periods with the peak excitation frequencies can be suggested in the figure, that is, the first-order natural period controlling stage, the second-order natural period controlling stage, and the transitional stage between them. At the first-order and second-order natural period stages, the sloshing periods are always around the corresponding sloshing natural periods. General speaking, the

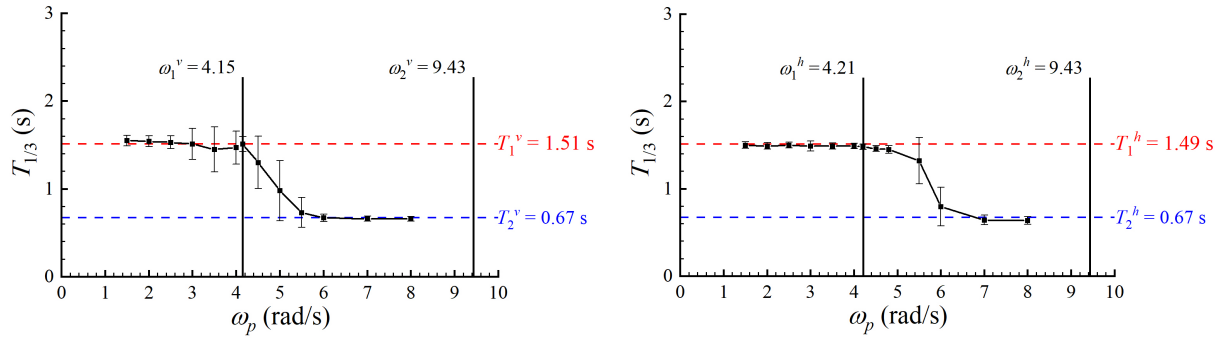

(a) Vertical baffle (b) Horizontal baffles

Figure 13: Statistical data of sloshing response periods in baffled tanks.

standard deviations are small, especially for the significant wave period $T_{1/3}$. This implies that the sloshing response mainly oscillates with the corresponding natural period. The decreased sloshing periods at the transitional stage can be observed with the increase of the peak frequency, where the standard deviations are generally large. The multiple-period oscillations in the sloshing response are the major reason for the phenomenon, implying the sloshing flow is controlled by two or more natural periods.

5.3. Influence of irregular excitation amplitude on sloshing responses

In this section, the influence of irregular excitation amplitude on the behavior of sloshing responses is investigated. As shown in Fig. 14, the histories of the wave elevation at the right corner with two amplitudes, $b_s = 0.002$ and 0.005 m, are illustrated, where the vertical and horizontal baffled tanks at $\omega_p = \omega_r$ are selected. The random variables are kept the same for the two external excitation amplitudes for the purpose of comparison. It is observed that the relative sloshing amplitudes at $b_s = 0.005$ is smaller than that at $b_s = 0.002$ m; while they have the same phase in the figure.

Fig. 15 shows the energy spectrum of sloshing responses, where two two excitation amplitudes of $b_s = 0.002$ and 0.005 m with three frequencies, $\omega_p = 0.50\omega_r$, $1.00\omega_r$, $1.50\omega_r$, are selected. It should be noted that the normalized time histories are adopted for the FFT analysis. Generally speaking, the energy spectrums at different excitation amplitudes b_s have the same characteristics, with the sloshing energy concentrated at the natural frequency or multiple natural frequencies. The peak values at $b_s = 0.005$ m are smaller than those at $b_s = 0.002$ m, implying the decreased relative sloshing response energy under larger excitation amplitudes b_s. This can be understood that the baffles, including both vertical and horizontal baffles, are able to generate more energy dissipation around the natural frequency for larger excitation amplitudes b_s. As for the frequencies far from the sloshing natural frequency, the insensitive effect of the excitation amplitude b_s on the energy spectrum can be observed.

The sloshing response amplitudes in the vertical and horizontal baffled tanks under different irregular excitation amplitudes are illustrated in Fig. 16. Again, the corresponding results under different regular excitation amplitudes are also included for the purpose of comparison. With the increase of regular excitation

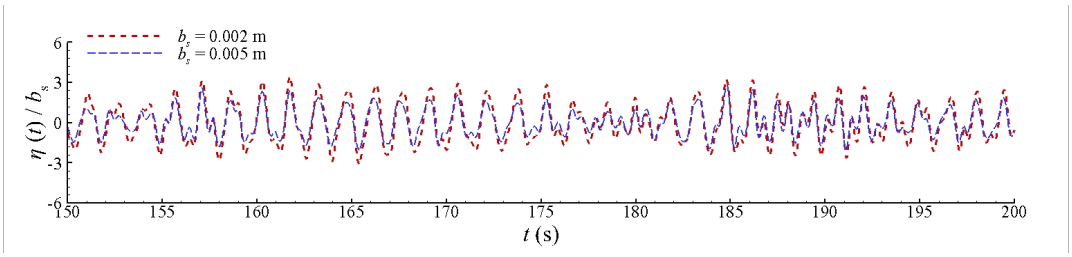

(a) Vertical baffle

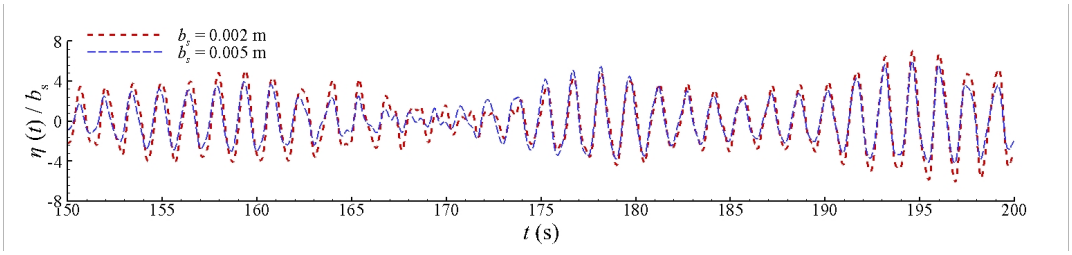

(b) Horizontal baffles

Figure 14: Time histories of the free surface elevation at the right side of the tank under different excitation amplitudes.

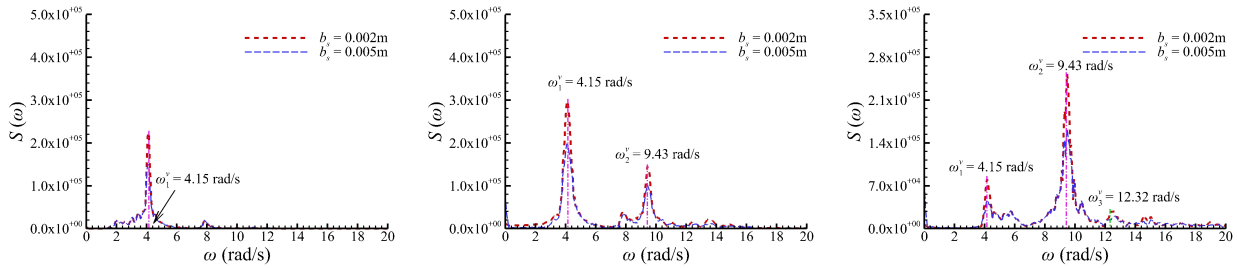

(a) $\omega_p = 0.50\omega_r$ (b) $\omega_p = 1.00\omega_r$ (c) $\omega_p = 1.50\omega_r$

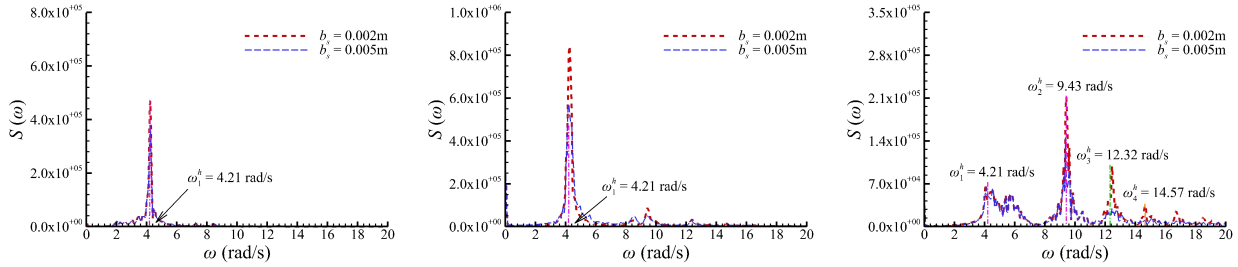

(d) $\omega_p = 0.50\omega_r$ (e) $\omega_p = 1.00\omega_r$ (f) $\omega_p = 1.50\omega_r$

Figure 15: Comparisons of sloshing response spectrums between $b_s = 0.002$ m and $b_s = 0.005$ m.

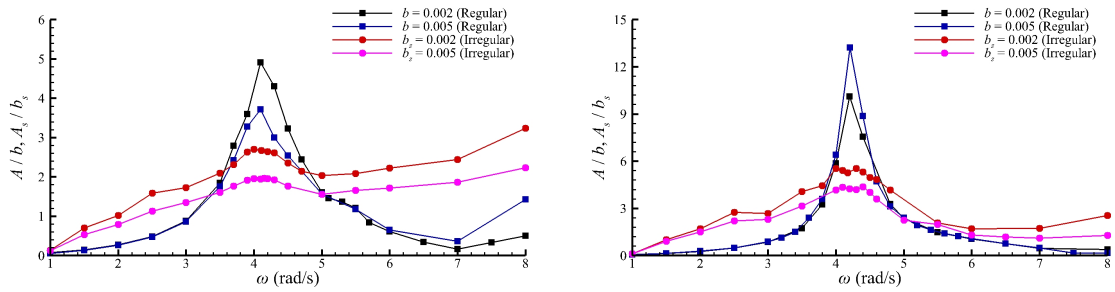

(a) Vertical baffle (b) Horizontal baffles

Figure 16: Influence of excitation amplitudes on the normalized sloshing response amplitudes.

amplitude, the normalized sloshing amplitude decreases around the sloshing natural frequency. While the decreased normalized sloshing amplitude can be observed across the entire range of irregular excitation frequencies. From the FFT results in Fig. 15, the sloshing responses under the irregular excitation are mainly contributed by the response components at the natural frequency, even when the ω_p is around the non-resonant frequencies. Therefore, the decreased response component at the natural frequency can lead to the decrease of sloshing amplitude under irregular excitations.

6. Conclusion

In this paper, a numerical model for viscous fluids is developed by using a computational fluid dynamics (CFD) method based on the Navier-Stokes equation, and the accuracy of the numerical model is validated by comparing with the available theoretical and numerical results. The liquid sloshing under irregular excitations is investigated, where the mechanism of sloshing responses is explained from the perspective of the statistical and spectral methods, which is also the major motivation of this study. The main conclusions are summarised as follows:

1) The ramp function applied during the starting stage of excitations is able to generate the steady-state results more rapidly when the excitation frequency is far from the resonant frequency. However, the initial transit is delayed by the ramp function when the excitation frequency is close to the resonant frequency. That is, the steady-state evolution is obtained more slowly when the ramp function is equipped at the resonant frequency.

2) The statistical results of $A_{1/3}$ and $A_{13\%}$ agree well with each other, indicating that the sloshing response under irregular excitations is consistent with the statistical characteristics of the Rayleigh distribution. The normalised sloshing amplitudes calculated from the samplings of the large free surface amplitudes are always smaller than the samplings of the small free surface amplitudes. That is, the value of $A_{1/10}/b_{1/10}$ is smaller than $A_{1/3}/b_{1/3}$; and A_{max}/b_{max} and A_{ave}/b_{ave} are the smallest and largest normalised sloshing amplitudes in the results, respectively.

3) The sloshing amplitudes in the tank by irregular excitations are smaller than those by regular excitations around the resonant frequency. Around the non-resonant frequencies, the irregular excitation results are larger than the regular excitation results, especially at the scope of the high-frequency range. Numerical analysis shows that the sloshing responses always oscillate around the natural frequencies even if the excitation spectral peak frequency is not close to the natural frequencies, because the natural frequencies are in the range of the excitation spectrum.

4) A three-phase variation of the sloshing response periods against the excitation peak frequencies can be suggested in this study, that is, the first-order natural period controlling stage, the second-order natural period controlling stage, and the transitional stage between them. At the first- and second-order natural period stages, the sloshing periods are always around the corresponding natural periods with small standard deviations. This is due to the fact that the sloshing response energy mainly concentrates at the corresponding sloshing natural frequencies. As for the transitional stage between them, the decreased sloshing periods with large standard deviations can be observed, where the sloshing response is controlled by two or more natural frequencies.

Acknowledgments

This work is supported by the Natural Science Foundation of China with Grant Nos. 52171250 and 51909027. The first author gratefully acknowledges the Supercomputer Center of Dalian University of Technology for providing computing resources.

References

Akyıldız, H., Ünal, N. E. and Aksoy, H. (2013). An experimental investigation of the effects of the ring baffles on liquid sloshing in a rigid cylindrical tank, *Ocean Engineering* **59**: 190–197.

Antuono, M. and Colagrossi, A. (2013). The damping of viscous gravity waves, *Wave Motion* **50**(2): 197–209.

Belakroum, R., Kadja, M., Mai, T. and Maalouf, C. (2010). An efficient passive technique for reducing sloshing in rectangular tanks partially filled with liquid, *Mechanics Research Communications* **37**(3): 341–346.

Biswal, K. C., Bhattacharyya, S. K. and Sinha, P. K. (2006). Non-linear sloshing in partially liquid filled containers with baffles, *International Journal for Numerical Methods in Engineering* **68**: 317–337.

Chen, B.-F. (2005). Viscous fluid in tank under coupled surge, heave, and pitch motions, *Journal of waterway, port, coastal, and ocean engineering* **131**(5): 239–256.

Cho, J. R., Lee, H. W. and Ha, S. Y. (2005). Finite element analysis of resonant sloshing response in 2-D baffled tank, *Journal of Sound and Vibration* **288**: 829–845.

Chu, C.-R., Wu, Y.-R., Wu, T.-R. and Wang, C.-Y. (2018). Slosh-induced hydrodynamic force in a water tank with multiple baffles, *Ocean Engineering* **167**: 282–292.

Faitinsen, O. M. et al. (1978). A numerical nonlinear method of sloshing in tanks with two-dimensional flow, *Journal of Ship Research* **22**(3): 193–202.

Faltinsen, O. M. and Timokha, A. N. (2001). An adaptive multimodal approach to nonlinear sloshing in a rectangular tank, *Journal of fluid mechanics* **432**: 167–200.

Faltinsen, O. M. and Timokha, A. N. (2002). Asymptotic modal approximation of nonlinear resonant sloshing in a rectangular tank with small fluid depth, *Journal of fluid mechanics* **470**: 319–357.

Hill, D. F. (2003). Transient and steady-state amplitudes of forced waves in rectangular basins, *Physics of Fluids* **15**(6): 1576–1587.

Hirt, C. W. and Nichols, B. D. (1981). Volume of fluid (VOF) method for the dynamics of free boundaries, *Journal of Computational Physics* **39**(1): 201–225.

Isaacson, M. and Subbiah, K. (1991). Earthquake-induced sloshing in a rigid circular tank, *Canadian Journal of Civil Engineering* **18**(6): 904–915.

Issa, R. I. (1986). Solution of the implicitly discretised fluid flow equations by operator-splitting, *Journal of Computational Physics* **62**(1): 40–65.

Jasak, H. (1996). *Error analysis and estimation for the finite volume method with applications to fluid flows*, PhD thesis, Imperial College London.

Jiang, S.-C., Bai, W. and Lan, J.-J. (2022a). Influence of a vertical baffle on suppressing sway motion response of a tank coupled with sloshing actions in waves, *Ocean Engineering* **260**: 111999.

Jiang, S.-C., Feng, A. and Yan, B. (2022b). Numerical simulations for internal baffle effect on suppressing sway-sloshing coupled motion response, *Ocean Engineering* **250**: 110513.

Jin, H., Liu, Y., Li, H. and Fu, Q. (2017). Numerical analysis of the flow field in a sloshing tank with a horizontal perforated plate, *Journal of Ocean University of China* **16**(4): 575–584.

Liu, D. and Lin, P. (2008). A numerical study of three-dimensional liquid sloshing in tanks, *Journal of Computational physics* **227**: 3921–3939.

Liu, D. and Lin, P. (2009). Three-dimensional liquid sloshing in a tank with baffles, *Ocean engineering* **36**: 202–212.

Lu, L., Jiang, S.-C., Zhao, M. and Tang, G.-Q. (2015). Two-dimensional viscous numerical simulation of liquid sloshing in rectangular tank with/without baffles and comparison with potential flow solutions, *Ocean Engineering* **108**: 662–677.

Luo, M., Koh, C. and Bai, W. (2016). A three-dimensional particle method for violent sloshing under regular and irregular excitations, *Ocean Engineering* **120**: 52–63.

Molin, B. and Remy, F. (2013). Experimental and numerical study of the sloshing motion in a rectangular tank with a perforated screen, *Journal of Fluids and Structures* **43**: 463–480.

Rafiee, A., Pistani, F. and Thiagarajan, K. (2011). Study of liquid sloshing: numerical and experimental approach, *Computational Mechanics* **47**: 65–75.

Rusche, H. (2003). *Computational fluid dynamics of dispersed two-phase flows at high phase fractions*, PhD thesis, Imperial College London.

Sanapala, V., Rajkumar, M., Velusamy, K. and Patnaik, B. (2018). Numerical simulation of parametric liquid sloshing in a horizontally baffled rectangular container, *Journal of Fluids and Structures* **76**: 229–250.

Sriram, V., Sannasiraj, S. and Sundar, V. (2006). Numerical simulation of 2d sloshing waves due to horizontal and vertical random excitation, *Applied Ocean Research* **28**(1): 19–32.

Wang, C. and Khoo, B. (2005). Finite element analysis of two-dimensional nonlinear sloshing problems in random excitations, *Ocean Engineering* **32**: 107–133.

Wu, G. X., Ma, Q. W. and Eatock Taylor, R. (1998). Numerical simulation of sloshing waves in a 3D tank based on a finite element method, *Applied ocean research* **20**: 337–355.

Xue, M.-A. and Lin, P. (2011). Numerical study of ring baffle effects on reducing violent liquid sloshing, *Computers & Fluids* **52**: 116–129.

Xue, M.-A., Zheng, J., Lin, P. and Yuan, X. (2017). Experimental study on vertical baffles of different configurations in suppressing sloshing pressure, *Ocean Engineering* **136**: 178–189.

Yu, L., Xue, M.-A. and Zheng, J. (2019). Experimental study of vertical slat screens effects on reducing shallow water sloshing in a tank under horizontal excitation with a wide frequency range, *Ocean Engineering* **173**: 131–141.

Yu, Y. X. and Liu, S. X. (2016). *Random wave and its applications to engineering. (In Chinese)*, Dalian University of Technology Press.